This article has been accepted for publication in IEEE Transactions on Power Electronics. This is the author's version which has not been fully edited and content may change prior to final publication. Citation information: DOI 10.1109/TPEL.2024.3355498

Equally Split PCB Inductor (ESPI) Design for High Energy Density and Low Near-Field Radiation

Ziyang Wang, *Member, IEEE*, Wucheng Ying, Yinong Zeng, Shuo Wang, *Fellow, IEEE*, Chaoqiang Jiang, *Member, IEEE*, Teng Long, *Member, IEEE*, Jian Qiu, Kefu Liu, *Member, IEEE*, and Hui Zhao, *Member, IEEE*

***Abstract*—PCB inductors can enhance the integration of power electronics systems, and hence are of high demand. Nevertheless, PCB inductors encounter challenges such as the severe skin effect and significant inductance reduction in both ac and dc condition as trace widths increase. This paper identifies the cause of this inductance reduction and proposes an innovative PCB inductor structure to mitigate these issues. The new design also utilizes split wires to effectively suppress the skin effect. Comprehensive simulations and experiments demonstrate that the proposed ESPI can achieve both high energy density and low near-field magnetic radiation. The design files, simulations, and experiment data are included in the multimedia folder.**

***Index Terms*—PCB inductors, optimized energy density, near-field radiation.**

I. Introduction

The growing demand for high integration in power electronics is driving the need for PCB integrated inductors. While there has been both notable research in both academia [1-5] and emerging industrial applications [6], existing PCB inductors still use similar structures as the structure of matured semiconductor-integrated designs as shown in Fig. 1. These conventional PCB inductors have not addressed challenges posed by high-current requirements in power electronics applications. Therefore, proposing a new structure to address these issues is crucial for PCB inductor design.

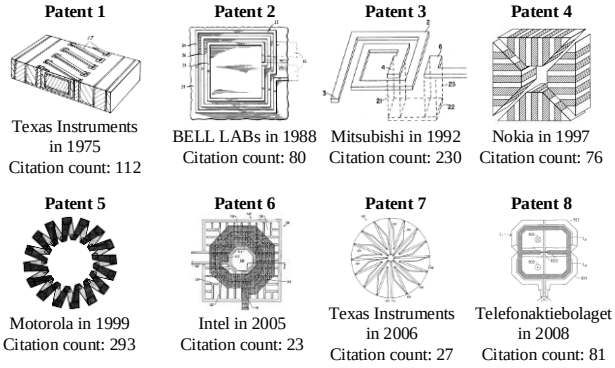

Fig. 1. Key patents for integrated inductors in the semiconductor industry (statistics up to November 2023). This extensive patent activity and widespread citations indicate the significance of integrated inductor technology in practical industrial applications.

Since 1975, the semiconductor industries have used on-chip integrated 2D inductors, as shown in Fig. 1. This extensive patent activity and widespread citations indicate the significance of integrated inductor technology in practical industrial applications. PCB inductors in power converters also pursue large inductance per unit area and high Q value, but there are also differences, e.g., PCB inductors use different conductor material, and have high current capacity requirements. Hence, it is necessary to evaluate if the structure of semiconductor inductors is suitable and ideal for PCB inductors.

Ref. [1, 2] extend the semiconductor integrated inductor structure from Patent 5 [7], and affirm the applicability of [7] for PCB inductors. Nevertheless, with increasing wire widths, notable inductance reduction and severe skin effect are observed. Ref. [3] introduces a planar litz structure inspired by the circular litz wires. However, the substantial extension of winding length significantly increases DC resistance (R_{dc}) and the number of vias. Using more vias increases manufacturing difficulty and reduces current capacity. Furthermore, to address the challenges in PCB inductor fabrication, ref. [4] implements 3D printing technology. Nevertheless, mass production costs of 3D printing are much higher than that of PCB inductor production. In 2023, [5] uses PCB inductors for buck converters, but these PCB inductors are still constructed like semiconductor integrated ones.

Recent advancements in PCB winding structures, as in [8-11], have primarily targeted the enhancement of Q value and AC loss reduction, yet the aspect of DC inductance remains unsolved. While [8] introduces a novel coil design for wireless power transfer, its impact on L_{dc} is minimal. Similarly, [9] delves into track width ratio optimization, again focusing on AC characteristics. Ref. [10] explores hollow windings for improved heat dissipation, enhancing AC loss and Q value without impacting L_{dc}. Ref. [11] focuses on electromagnetic analysis of ferrite-core inductors, but not applicable to air-core PCB inductors. This underscores the need for further

Ziyang Wang, Yinong Zeng, Jian Qiu, Kefu Liu, and Hui Zhao are with the Department of Illuminating Engineering and Light sources, Institute for Electric Light Sources, Fudan University, Shanghai 200433, China (e-mail: 22210720049@m.fudan.edu.cn; ynzeng21@m.fudan.edu.cn; jqiu@fudan.edu.cn; kfliu@fudan.edu.cn; hui_zhao@fudan.edu.cn).

Wucheng Ying and Teng Long is with the Electrical Engineering Division, Department of Engineering, University of Cambridge, CB2 1TN Cambridge, U.K. (e-mail: wy256@cam.ac.uk; tl322@cam.ac.uk).

Shuo Wang is with the Electrical and Computer Engineering, University of Florida, Gainesville, FL 32611-7011 USA (e-mail: shuowang@ieee.org).

Chaoqiang Jiang is with the Department of Electrical Engineering, City University of Hong Kong, China (email: chjiang@cityu.edu.hk).

exploration in PCB inductor design, specifically aimed at resolving inductance reduction issues in both DC and AC conditions.

Besides the mentioned engineering practices, [12] introduces calculation formulae for different shape inductors. Ref. [13] further discusses the optimal structure for inductors based on various scenarios, ultimately asserting that the optimal inductor configuration is contingent upon dimensions. However, refs. [12, 13] are still based on the conventional semiconductor inductor structures and have not yet uncovered the cause nor resolve the issues pertaining to PCB inductors. Consequently, investigating the suitable PCB inductors' structure becomes imperative.

This paper identifies the cause of this inductance reduction both in DC and AC conditions and proposes an innovative PCB inductor structure to mitigate this issue. The proposed design also utilizes the split wire to effectively suppress the skin effect. Comprehensive simulations and experiments demonstrate that this proposed inductor can achieve both high energy density and low radiation.

II. Existing Methods and Issues in PCB Inductor Design

A. Inductor Design: from Semiconductors to PCB

Transplanting semiconductor 2D inductors to PCB is mature. Firstly, the inductor structure remains unchanged and is directly ported to the PCB. Then increase the trace width and copper thickness of the inductor to achieve a larger current carrying capacity. The process is as shown in Fig. 2.

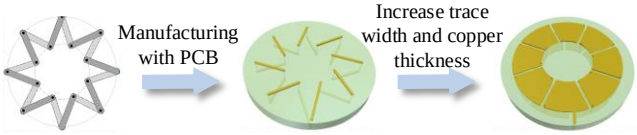

Fig. 2. Existing method of transplanting semiconductor 2D inductors onto PCBs. This approach has been validated by various researches [1, 2, 4].

B. Issues: Severe Skin Effect and Inductance Reduction with Wide Traces

This simple transplantation method has two issues. Firstly, under high-frequency conditions, PCB conductors induce notable skin effect, leading to higher losses and lower Q value. In semiconductor processes, copper is chosen for PCBs due to superior conductivity, but its smaller skin depth, causes more pronounced skin and proximity effects.

Besides, the method of widening the trace is equally problematic even at low frequencies. Clayton R. Paul provided the fundamental formula for a single-turn coil in [14] as (1). A plot of the inductance of a single-turn coil against the width of the conductor can be shown as Fig. 3.

$$L_{rec}=\frac{\mu_0}{\pi}\left[\begin{array}{l}-l\ln\left(1+\sqrt{1+\left(\frac{w}{l}\right)^2}\right)-w\ln\left(1+\sqrt{1+\left(\frac{l}{w}\right)^2}\right)\\ +l\ln\left(\frac{2w}{r/2}\right)+w\ln\left(\frac{2l}{r/2}\right)+2\sqrt{l^2+w^2}-2(w+l)\end{array}\right] \quad (1)$$

$l, w \gg r$

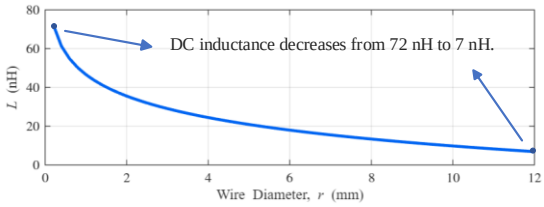

Fig. 3. Inductance decreases as radius increases. Denoting l as the width of rectangular coil, w as the length of rectangular coil, r as the diameter of the coil wire. When $w = l = 20$ mm, r increases from 0 to 12 mm. It means higher currents necessitate wider conductors, but this leads to a reduction in inductance.

Litz wire is commonly employed to ensure that the dimensions of each wire are significantly smaller than the skin depth, therefore effectively mitigating skin effect at high frequencies. However, the issue of decreasing inductance, as indicated by (1) and Fig. 3, remains unresolved. Furthermore, litz wires have limitations in terms of integration, as their degree of twisting and insulation control can be challenging. Additionally, the employment of round wires in litz configurations also tends to result in considerable volume inefficiency.

III. Proposed Inductor Structure

A. Physical Explanation of Inductance Decreasing

Fig. 4 illustrates the most direct mechanism behind the phenomenon of inductance decreasing. The innermost layer of the circuit has the shortest path and lowest resistance, causing a concentration of current and charge in the innermost. This phenomenon leads to a reduction in the loop area of the inductor, resulting in a decrease in the inductance value.

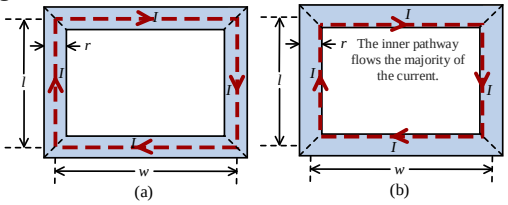

Fig. 4. Structure of rectangular loop inductor. (a) Usually expected current distribution. (b) Actual current distribution: concentrated in the innermost part. Therefore, the actual area enclosed by the current is reduced, and the inductance is reduced with trance width increasing.

B. Splitting Wires Procedure

In order to suppress skin effect, the wide wire need to be split into thin conductors as shown in Fig. 5(b). The design flowchart is as shown in Fig. 6, and the principles of the design are as follows:

1) Spacing, w_{sp}: w_{sp} is determined by the capability of the PCB manufacture.

2) Width, w: w is determined with the target frequency to suppress the skin effect. Denoting ρ as the electrical conductivity of copper, μ as the magnetic permeability of copper, t as the thickness of copper, and f as the operating frequency of the system. The AC resistance formula [15] is given in (2), where we normally consider that a rise in R_{ac} of no more than 2% is sufficient to represent freedom from skin effects:

$$R_{ac\_rec}/R_{dc\_rec}=\left[K_C/(1-e^{-x})\right]\le 1.02 \quad (2)$$

This article has been accepted for publication in IEEE Transactions on Power Electronics. This is the author's version which has not been fully edited and content may change prior to final publication. Citation information: DOI 10.1109/TPEL.2024.3355498

where

$$\begin{cases} K_C = 1+\left(1-e^{\frac{-0.026(wt)^{0.5}}{1.26\sqrt{\rho/(\pi f \mu)}}}\right)\left[1.2/e^{2.1t/w}+1.2/e^{2.1w/t}\right] \\ x = 2\sqrt{\rho/(\pi f \mu)}/t(1+t/w)+8(\sqrt{\rho/(\pi f \mu)}/t)^3/(w/t) \end{cases}$$

3) Count of wires, N_w: N_w is limited by the size limitation. Denoting W_{total} as the total width requirement, the N_w is limited by:

$$N_w \le 1/4\left(W_{total}/\left(w+w_{sp}\right)+1\right) \quad (3)$$

C. Equalizing Split Wires Procedure

In order to further solve the problem of inductance decrease caused by wide wire, it is necessary to rotate wires from top to bottom layer. The serpentine curve is utilized to ensure the perfect consistency in length of split wires so that the inductance of each wire is as identical as possible. The design is shown in Fig. 5(c). The principles of the design are as follows:

1) Vias should take on the role of position rotating: after passing through the vias, the outermost alignments should be rotated to the innermost; and the innermost alignments should be switched to the outermost in order to ensure the general symmetry of the alignment of length.

2) Serpentine alignment should be utilized to compensate for the alignment with unequal length. After the proposed design, the lengths of segments of the inductor are recorded in Table I and are exactly the same.

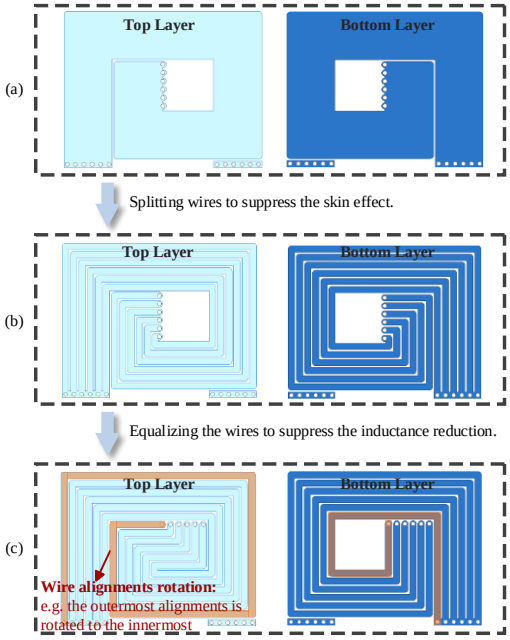

Fig. 5. Three PCB planar inductor structures: (a) existing wide wire structure, (b) improved split wire structure, (c) the proposed ESPI. All three inductors are the same size and thickness, and the same manufacturing process and manufacturer have been chosen.

The new structure of the inductor can effectively avoid the concentration of current on the inner side and improve the high frequency characteristics of the inductor. In Section IV, Fig. 7 and Fig. 8 verifies the distribution of current, Fig. 9 and Fig. 11 verifies the magnitude of radiation produced, and Fig. 12 verifies the trend of inductance variation, all of which are consistent with theoretical expectations.

TABLE I
LENGTH OF EACH SEGMENT OF INDUCTOR IN FIG. 5(C)

No. of wire	Top Layer ($l-l_{grid}$ * 1.186 mm)							Bottom Layer ($l-l_{grid}$ * 1.186 mm)							Serpentine Winding Section ($l-l_{grid}$ * 1.186 mm)	Total Length ($l-l_{grid}$ * 1.186 mm)
	Length of Each Segment						Total Length	Length of Each Segment						Total Length		
1	18	23	17	17	11	6	92	6	7	7	13	13	46	0	138
2	17	21	15	15	9	6	83	7	9	9	15	14	54	1	138
3	16	19	13	13	7	6	74	8	11	11	17	15	62	2	138
4	15	17	11	11	5	6	65	9	13	13	19	16	70	3	138
5	14	15	9	9	3	6	56	10	15	15	21	17	78	4	138
6	13	13	7	7	1	6	47	11	17	17	23	18	86	5	138

D. Design Flowchart

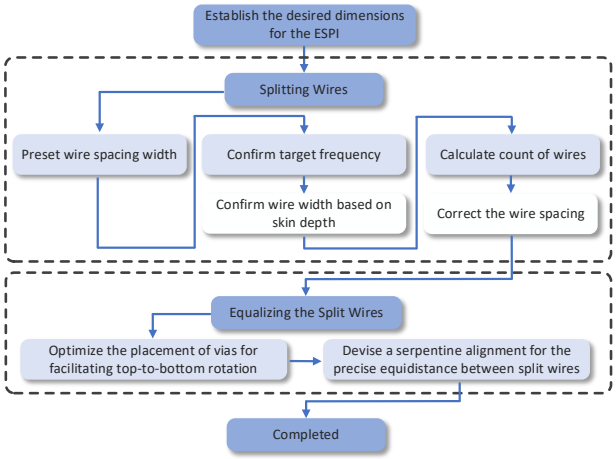

Fig. 6. Flowchart for the design of the proposed ESPI. The derivation of specific equations for the calculation of inductance is included in multimedia folder.

IV. SIMULATION AND EXPERIMENTAL RESULTS

A. Comparison of Current Distributions

Fig. 7 and Fig. 8 compare the current distribution of the proposed ESPI and the commercialized inductor from Coilcraft, as well as PCB inductors with wide wire and split wires. The proposed ESPI has the best current distribution.

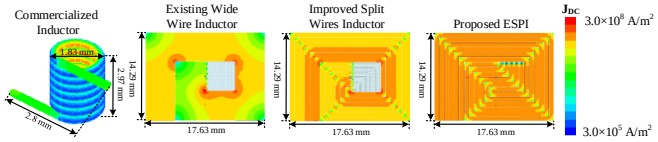

Fig. 7. Comparison of the simulated current distribution @ DC condition. Split wires inductor improves current distribution, but still concentrates more on the inner wires due to unequal lengths of split wires. The proposed ESPI has the most uniform current distribution. Simulations are included in the multimedia folder.

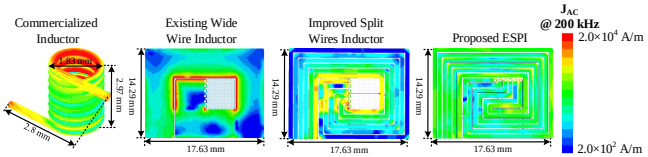

Fig. 8. Comparison of the simulated current distribution @ 200 kHz. Split wires inductor suppresses skin and proximity effects, but the problem of unequal wire lengths still hurts the AC current distribution. Therefore, the proposed ESPI has the most uniform current distribution. Simulations are included in the multimedia folder.

This article has been accepted for publication in IEEE Transactions on Power Electronics. This is the author's version which has not been fully edited and content may change prior to final publication. Citation information: DOI 10.1109/TPEL.2024.3355498

B. Comparison of Magnetic Field Distributions

Fig. 9 compares the radiation results of three PCB inductors and the commercialized inductor. Experiment in Fig. 10 verifies the accuracy of electromagnetic simulations. The comparison results are shown in Fig. 11. The radiation results of simulation and experiment are matched.

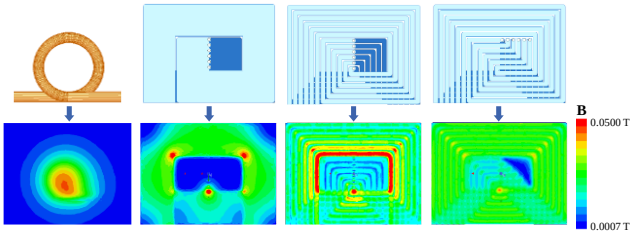

Fig. 9. Comparison of the simulated radiation values at 0.1 mm height with 100 A current. The distribution of magnetic field strength of the split wires inductor is more uniform than that of the wide wire inductor, but not as uniform as the ESPI. The proposed ESPI yields a more uniform magnetic field distribution with a smaller maximum value of the magnetic field strength. Simulations are included in the multimedia folder.

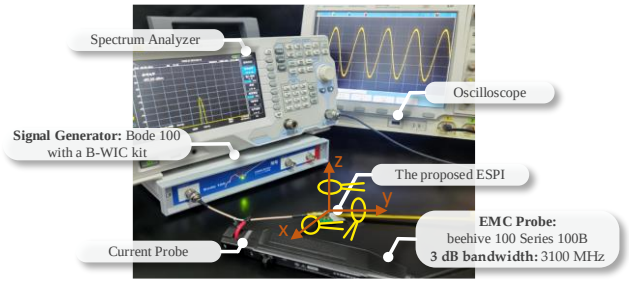

Fig. 10. Radiation measurement test bench setup. The Bode 100 with fixed frequency serves as the signal generator, which is connected to an oscilloscope to monitor through a current probe. The effective input current set at 40 mA. Coordinate paper is affixed to the proposed ESPI to measure radiation at equidistant points. The EMC probe, specifically the beehive 100 Series 100B, is used to measure the radiation components in the x, y, and z directions. The root mean square (RMS) value of these measurements is taken as the final total radiation value. The EMC probe is connected to a spectrum analyzer, which reads and records the measurement results. Raw data for the experiment is shown in multimedia folder.

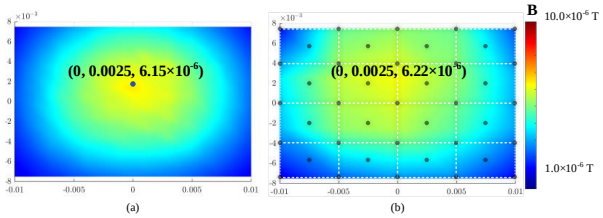

Fig. 11. Comparison of simulated and experimental radiation values at 4.6 mm height with 40 mA current: (a) simulation result, and (b) experiment result. The coordinate paper is segmented into 5*5 = 25 sections, to conduct the radiation measurements. For each grid section, radiation data is collected at four corner points and the central point to ensure comprehensive coverage and accurate image fitting. Simulated and experimental results of radiation distribution are welly matched. The error at the radiation maximum point is 1.12%.

C. Comparation of Inductance, Resistance and Q value

Fig. 12 gives the simulation results of Q3D in terms of parameter extraction. The proposed ESPI performs optimally in terms of AC resistance, inductance and *Q* value. The DC resistance value of the proposed ESPI in Fig. 12(a) is higher compared to the other two structures. This is due to the fact that splitting causes a decrease in the cross-sectional area of the conductor and the current cannot flow from the innermost side at corners. Besides, equalizing causes the total length of the conductor to rise. Fig. 13 demonstrates that simulated and experimental results of impedance measurement are welly matched.

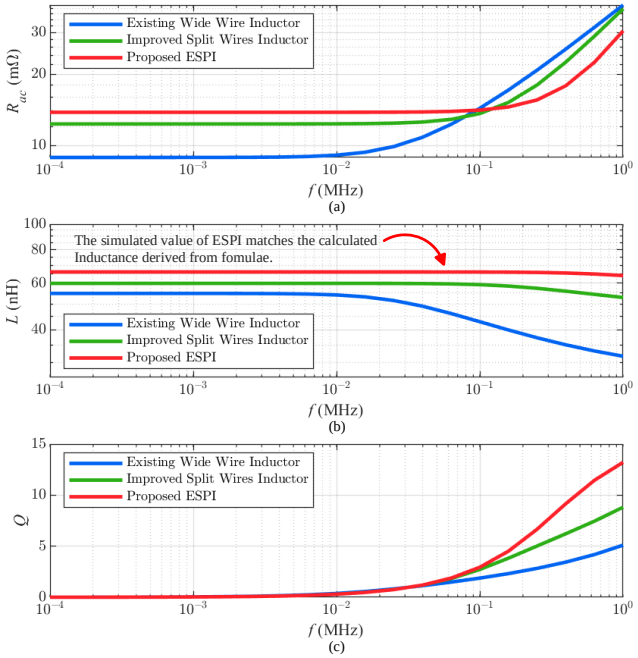

Fig. 12. Q3D simulation parameter results of three PCB inductors: (a) resistance; (b) inductance; (c) *Q* value.
Existing Wide Wire Inductor: a serious skin effect and poor inductance characteristics in both DC and AC conditions.
Improved Split Wires Inductor: mitigate the skin effect and have a noticeable increase in L_{ac} and *Q* value compared to wide wire inductor. However, the DC inductance hasn't improved significantly because of uneven current distribution.
The proposed ESPI: not only solves the AC effect, but DC inductance continues to increase compared to split wires inductor. Therefore, the proposed ESPI exhibits the highest *Q* value, aligning well with theoretical predictions.
Simulations and derivation of specific equations for the calculation of inductance are included in the multimedia folder.

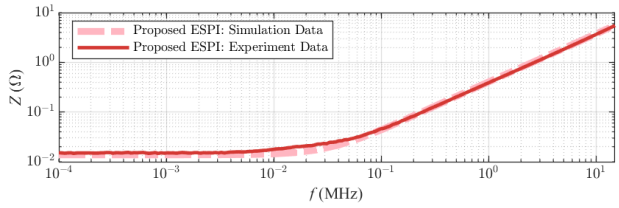

Fig. 13. Comparison of simulated and experimental results for impedance. The simulated and experimental results of impedance measurement are welly matched.

D. Experiment of Thermal Distribution

Fig. 14 gives a photograph of the ESPI and the thermal distribution under actual circuitry with a 20 ℃ temperature rise, demonstrating the excellent heat dissipation capability of its 2D structure and the feasibility of its practical application. The ESPI has a current carrying capacity of 4.0 A at a 20 ℃ temperature rise.

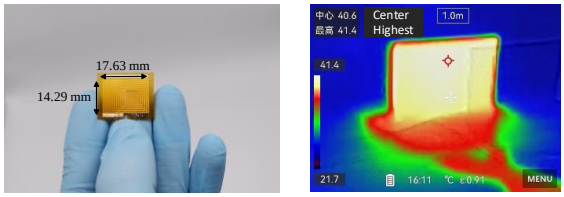

(a) (b)

Fig. 14. (a) The photo of the proposed ESPI, (b) experimental result of 4.0 A current at 20 ℃ temperature rise.

TABLE II provides a comparison of key electrical parameters for three different inductors. The proposed ESPI inductor showcases a superior energy density of 22.06×10^{-9} J/mm³, which means a 27% increase over the commercial inductor and a substantial 513% increase over the litz-wire-based inductor. The proposed ESPI also achieves a compact volume and comparable inductance and current-carrying capabilities. This multi-faceted superiority makes the ESPI an attractive option for applications where integration, efficiency, and energy density are critical considerations.

TABLE II
COMPARISON OF COMMERCIALIZED INDUCTOR LITZ-WIRE-BASED INDUCTOR AND THE PROPOSED ESPI

	Commercial Air-core Solenoid Inductor 0908SQ-27N (2 in series)	Litz-wire-based Inductor	The Proposed ESPI
Inductance @ 200 kHz (nH)	27.3*2=54.6	59.1	66
DC Resistance (mΩ)	10*2=20	8.3	14
Volume (mm^3)	2.97*1.83*2.8*2=30.44	5.3*5.3*12.2=342.7	17.63*14.29*0.095=23.94
Current @ 20 ℃ rise (A)	4.4	6.5	4.0
Energy Density ($10^{-9}\times J/mm^3$)	17.36	3.6	22.06

V. CONCLUSION

In conclusion, this research addresses the need for high-performance PCB inductors and have several achievements:

Identification of the Cause of DC Inductance Reduction: this manuscript uncovers and identifies the underlying cause of inductance reduction and give the physical explanation.

Innovative Structure: a novel PCB inductor structure has been proposed, effectively suppressing both the skin effect and inductance reduction, to design inductor with high-current capacity and high-energy density.

Comprehensive Equations: this study provides comprehensive equations that model the behavior of PCB inductors under various conditions, enabling precise design and optimization. The calculation result using simplified equations is 66.0882 nH, with an error of 0.07% from simulated value. The derivation of specific equations for the calculation of inductance are included in the multimedia folder.

Design Flowchart: a structured design flowchart has been established to guide the development of high-performance PCB inductors.

High Energy Density and Low Radiation: the proposed PCB inductor design has been validated through both simulations and experiments. The energy density and radiation level are better than that of both conventional PCB inductors and commercialized products.

Optimal Thermal Performance: additionally, our design exhibits excellent thermal performance, ensuring stable operation under demanding high-current.

ACKNOWLEDGMENT

The authors would like to express their gratitude to Dr. Yiming Li of Monolithic Power Systems (MPS) for his invaluable advice during the revision of Fig. 5. We also extend our heartfelt thanks to Yi Du, Rongrong Zhang, Pengyao Xie for their invaluable assistance with the experimental aspects of this research. Additionally, we had the pleasure of discussing these ideas with Dr. Handong Gui when we were at the University of Cambridge. We sincerely thank Dr. Gui for his encouragement and are sorry that we are not able to work together.

REFERENCES

[1] M. Biglarbegian, N. Shah, I. Mazhari, J. Enslin, and B. Parkhideh, "Design and evaluation of high current PCB embedded inductor for high frequency inverters," 2016 IEEE Applied Power Electronics Conference and Exposition (APEC), pp. 2998-3003, 2016, doi: 10.1109/APEC.2016.7468290.

[2] S. Orlandi et al., "Optimization of Shielded PCB Air-Core Toroids for High-Efficiency DC–DC Converters," IEEE Transactions on Power Electronics, vol. 26, no. 7, pp. 1837-1846, 2011, doi: 10.1109/tpel.2010.2090902.

[3] S. Wang, M. A. deRooij, W. G. Odendaal, J. D. vanWyk, and D. Boroyevich, "Reduction of High-Frequency Conduction Losses Using a Planar Litz Structure," *IEEE Transactions on Power Electronics*, vol. 20, no. 2, pp. 261-267, 2005, doi: 10.1109/tpel.2004.843022.

[4] L. Wei, R. Luke, and J. Rivas, "3-D-Printed Air-Core Inductors for High-Frequency Power Converters," *IEEE Transactions on Power Electronics*, vol. 31, no. 1, pp. 52-64, 2016, doi: 10.1109/TPEL.2015.2441005.

[5] Y. Kandeel, S. O'Driscoll, C. O'Mathuna, and M. Duffy, "Optimum Phase Count in a 5.4-W Multiphase Buck Converter Based on Output Filter Component Energies," *IEEE Transactions on Power Electronics*, vol. 38, no. 4, pp. 4909-4920, 2023, doi: 10.1109/tpel.2022.3226708.

[6] Infineon, "1.1 kW 48 V to 12 V zero-voltage switching switched capacitor converter (ZSC) with XDPP1100 controller," AN_2301_PL88_2302_214945 datasheet, Feb. 2023.

[7] R. C. Alford, "Method of forming a three-dimensional integrated inductor," Dec. 28, 1999.

[8] C. M. Awuah, P. Danuor, J. I. Moon, and Y. B. Jung, "Novel coil design and analysis for high-power wireless power transfer with enhanced Q-factor," *Sci Rep*, vol. 13, no. 1, p. 4187, Mar 14 2023, doi: 10.1038/s41598-023-31389-y.

[9] S. R. Cove and M. Ordonez, "Wireless-Power-Transfer Planar Spiral Winding Design Applying Track Width Ratio," *IEEE Transactions on Industry Applications*, vol. 51, no. 3, pp. 2423-2433, 2015, doi: 10.1109/tia.2014.2372092.

[10] S. R. Cove, M. Ordonez, N. Shafiei, and J. Zhu, "Improving Wireless Power Transfer Efficiency Using Hollow Windings With Track-Width-Ratio," *IEEE Transactions on Power Electronics*, vol. 31, no. 9, pp. 6524-6533, 2016, doi: 10.1109/tpel.2015.2498638.

[11] R. Zhang, S. Wang, T. Long, J. Qiu, K. Liu, and H. Zhao, "The Magnetized Capacitance, First Resonant Frequency, and Electromagnetic Analysis of Inductors With Ferrite Cores," *IEEE Transactions on Industrial Electronics*, pp. 1-11, 2023, doi: 10.1109/tie.2023.3294611.

[12] M. d. M. H. Sunderarajan S. Mohan, Stephen P. Boyd, and Thomas H. Lee, "Simple accurate expressions for planar spiral inductances," *IEEE Journal of Solid-State Circuits*, vol. 34, no. 10, pp. 1419-1423, 1999, doi: 10.1109/4.792620.

[13] J. M. Lopez-Villegas, N. Vidal, and J. A. del Alamo, "Optimized Toroidal Inductors Versus Planar Spiral Inductors in Multilayered Technologies," *IEEE Transactions on Microwave Theory and Techniques*, vol. 65, no. 2, pp. 423-431, 2017, doi: 10.1109/tmtt.2016.2645571.

[14] C. R. PAUL, *Inductance: Loop and Partial*. NJ: Wiley, 2011.

[15] A. Payne, "The AC Resistance of Rectangular Conductors," 2021.